

PHYSICAL CHEMISTRY  
OF NANOCCLUSERS AND NANOMATERIALS

## Synthesis, Structure, and Physical Properties of a Nanocomposite Based on Graphene Oxide and TiO<sub>2</sub>

N. Kh. Ibrayev<sup>a,\*</sup>, E. V. Seliverstova<sup>a,\*\*</sup>, A. E. Sadykova<sup>a</sup>, and T. M. Serikov<sup>a</sup>

<sup>a</sup>*Institute of Molecular Nanophotonics, Buketov Karaganda University, Karaganda, 100028 Kazakhstan*

\* *e-mail: niazibrayev@mail.ru*

\*\* *e-mail: genia\_sv@mail.ru*

Received May 12, 2020; revised May 12, 2020; accepted June 6, 2020

**Abstract**—The influence of the graphene oxide addition on the structural, optical, optoelectronic and photovoltaic properties of TiO<sub>2</sub> was studied. It was shown that a nanocomposite material is formed during hydrothermal synthesis; this fact was proven by the data obtained by electron microscopy and XPS analysis. It was estimated that the absorption spectrum of the TiO<sub>2</sub>–GO nanocomposite is shifted to the longwave region as compared to the absorption spectra of the initial components. The data on the quenching of luminescence of the synthesized material evidence that the efficiency of the recombination processes of photogenerated electron–hole pairs is lower as compared to pure TiO<sub>2</sub>; it improves the photoelectric, photovoltaic and electro-physical parameters of TiO<sub>2</sub>–GO nanocomposite material.

**Keywords:** nanocomposite, graphene oxide, titanium dioxide, structure, current–voltage characteristics, photovoltaics

**DOI:** 10.1134/S0036024421040105

Graphene is a very attractive material for the development of the graphene-containing inorganic composites due to its electronic properties, high transparency, mechanical characteristics, and high specific surface. Several methods are used for obtaining graphene; graphite oxidation (the Hummers' method) that leads to the formation of graphene oxide (GO) is the most popular among them [1, 2].

GO is more convenient for technological use than graphene, because GO forms stable dispersions in water and certain organic solvents [3, 4]. In addition, its optical, conducting, and chemical properties can be changed by the reduction of graphene oxide and variation of the content of oxygen-containing groups, such as functional carboxyl, hydroxyl, and epoxide groups [5, 6]. It also provides the possibility of controlling the band gap of graphene oxide [7]; such a possibility is very urgent for GO use in the organic photovoltaics, photocatalysis, electronics, and optoelectronic devices and in combination with other inorganic materials.

For example, GO–semiconductor nanocomposite structures demonstrate enhanced optical, photocatalytic, and photodetecting properties as compared to the initial materials [5, 8, 9]. Titanium dioxide, which is widely used in photocatalysis for the degradation of organic compounds, water splitting, and as an active material for UV photodetectors [10, 11], should be mentioned among the most frequently used metal

oxide semiconductors. The use of TiO<sub>2</sub> in photovoltaic cells is also very popular due to its chemical stability, optical characteristics, and band structure, which is compatible with numerous organic sensitizer dyes.

Currently, a lot of effort is aimed at the improvement of the efficiency of organic solar cells. The main methods for the solution of this problem are the development of new materials and improvement of the efficiency of phototransformation and charge transport characteristics of the components that have already been used. Graphene and its derivatives can be used for it.

Particularly, it was shown in [12, 13] that graphene photoanodes improve the fill factor of solar cells, but lower the efficiency of solar devices. Besides, graphene films were used as withdrawal electrodes [14]; at this, the efficiency of the obtained cells varied within 0.5–7.5%. The films based on the mixture of graphene/graphene oxide and titanium oxide were used as photoanode of the Grätzel cells in the studies [15–17]. It was shown that photovoltaic parameters are improved generally, due to the change of the optical characteristics of the obtained samples and lowering of the recombination processes in the semiconducting film. However, the use of the nanocomposite material synthesized by the hydrothermal method has almost not been reported.

In this study, we show that the formation of a nanocomposite material based on graphene oxide and TiO<sub>2</sub>

that is characterized by better photoelectric and photovoltaic parameters as compared to pure  $\text{TiO}_2$  is provided by a hydrothermal reaction.

## EXPERIMENTAL

A nanocomposite based on GO and  $\text{TiO}_2$  was synthesized by a hydrothermal method according to the technique given in [5, 9]. GO (SLGO, Cheaptubes) and  $\text{TiO}_2$  (nanoparticles diameter of  $\sim 21$  nm, anatase, 99.7%, Sigma Aldrich), deionized water purified using AquaMax water purification system, and ethanol (anhydrous) were used for the preparation of nanocomposite. All reagents were of the analytical grade; they were used without further purification. GO concentration in composite was 5 wt % with respect to the amount  $\text{TiO}_2$ , because we previously showed that the highest effect on the charge transport parameters and photocatalytic activity of the synthesized nanocomposite is observed at this concentration [5].

The films of  $\text{TiO}_2$  or nanocomposite were applied onto the surface of glass substrates coated with conductive FTO layer (Fluorine doped tin oxide coated glass slide,  $\sim 7 \Omega/\text{sq}$ , Sigma Aldrich) by centrifuging at the rate of 1000 rpm from the ethanol paste to measure the optoelectronic parameters. The films were formed on the quartz substrates to conduct the optical measurements.

The morphology of the surface and microstructure of the obtained composite materials were studied using a Tescan Mira-3 scanning electron microscope (SEM) and JEM-2100F (Jeol) transmission electron microscope (TEM) at the accelerating voltage of 200 kV.

Structural properties of the synthesized nanocomposites were studied by the X-ray photoelectron spectroscopy (XPS). XPS spectra were registered using Axis Ultra DLD spectrometer (Kratos Analytical) at the transmission energy of 160 eV (overview spectrum) and 40 eV (high-resolution spectra). The spectra were registered using  $\text{AlK}_\alpha$  X-ray source with neutralizer. Spectra were calibrated against  $\text{Ti } 2p_{3/2}$  at 458.6 eV. The spectra of GO sample were calibrated using  $\text{O } 1s$  line at 532.5 eV.

Absorption and luminescence spectra were registered using Cary-300 and Eclipse (Agilent) spectrometers, respectively. The samples were placed into the optical cryostat (Oxford Instr.) for the measurements. The band gap was estimated using the technique given in [9, 18], by plotting a tangent to the edge of the absorption band of semiconductor and determining the point of its intersection with the abscissa axis. The error in determination of the band gap is  $\pm 0.01$  eV.

The current–voltage characteristics (CVC) of the prepared samples were registered using Elins P-20X

potentiostat/galvanostat (Elins). The samples were irradiated with xenon lamp ( $35 \text{ mW}/\text{cm}^2$ ).

Glass substrates coated with an FTO layer were used for the preparation and assemblage of solar cells. A blocking layer of  $\text{TiO}_2$  was applied onto the FTO surface according to the technique given in [19, 20]. The thickness of the obtained films was measured by SEM ( $10\text{--}12 \mu\text{m}$ ). Solar cells were sensitized by ruthenium dye N719 (Sigma Aldrich). Then the platinum electrodes were separately prepared on the FTO surface. Platinum was electrodeposited from the solution of  $\text{H}_2\text{PtCl}_6$  (Sigma Aldrich) in ethanol. The assemblage of cells was completed at the final stage using the standard technique given in [20].

Photovoltaic parameters were determined by the irradiation of the cells with the xenon lamp light at the radiation power of  $100 \text{ mW}/\text{cm}^2$  using Cell Tester Model CT50AAA (Photo Emission Tech., Inc., USA). The value of efficiency of solar cells was determined using the obtained values of open-circuit voltage, short-circuit current, and fill factor. ZView 3.2b software and equivalent circuit were used to analyze the data obtained with Z500PRO impedance meter.

## RESULTS AND DISCUSSION

An overview of the XPS spectra of the studied samples are given in Fig. 1. The lines attributed to carbon, oxygen, and titanium are observed in the spectra. The energy calibration of the spectra of the titanium-containing samples was performed using  $\text{Ti } 2p_{3/2}$  line. The observed position of the line corresponding to C–C bonds in the adsorbed carbon-containing compound was  $\sim 285.0$  eV at such calibration. The shape of  $\text{Ti } 2p$  XPS spectra was almost identical for all samples; it evidences the identical state of titanium in the samples.

Figure 1 shows that  $\text{C } 1s$  spectra of  $\text{TiO}_2$ –GO samples cannot be described as a sum of  $\text{TiO}_2$  and GO spectra. Two types of peaks can be marked out at the decomposition of spectra: the ones related to the oxygen-containing groups (at the region of 286.7 and 288.4 eV) and the ones attributed to the different states of carbon atoms. At this, one asymmetrical component corresponds to the spectrum of the  $sp^2$  hybridized carbon ( $\sim 284$  eV), while the symmetrical components were used to describe other states. The observed energy of the bond of the  $sp^2$  hybridized carbon ( $\sim 283.6$  eV) is significantly lower than the typical bond energy (usually of  $\sim 284.3\text{--}284.5$  eV). Such a shift can be related to the differential charging of the conductive particles of the  $sp^2$  hybridized carbon with respect to the nonconducting  $\text{TiO}_2$  matrix. Authors of [21, 22] also mention that such a shift evidences the chemical binding between GO and  $\text{TiO}_2$ . Besides, the shoulder at  $\sim 283.6$  eV is more pronounced in the spectrum of  $\text{TiO}_2$ –GO; the fraction of C–O and C=O bonds sig-

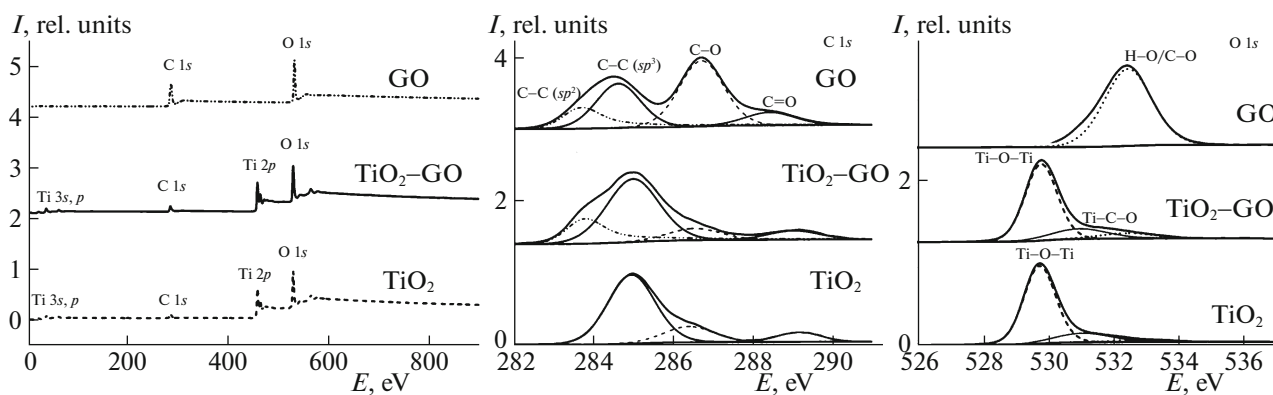


Fig. 1. XPS spectra of GO, TiO<sub>2</sub>, and TiO<sub>2</sub>-GO nanocomposite.

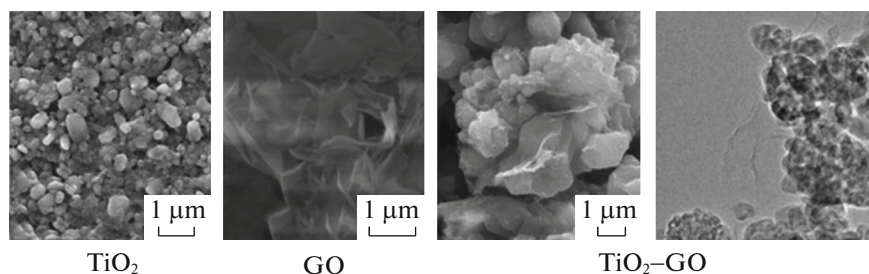


Fig. 2. SEM and TEM (rightmost) images of TiO<sub>2</sub>, GO, and TiO<sub>2</sub>-GO.

nificantly decreases (see the decrease of the integrated areas of these spectra, Table 1). It evidences the fact that the reduction of graphene oxide takes place in the nanocomposite material; the fraction of the  $sp^2$  hybridized carbon is higher. It is also proven by the values of areas below the curves with maximum at 283.6 eV that are equal to 1.17 and 0.64 rel. units for GO and TiO<sub>2</sub>-GO, respectively.

The obtained results accord with our structural analysis data [5, 9] obtained by IR spectroscopy and the decrease of the content of the oxygen-containing bonds.

O 1s spectra of the studied samples (except GO) are characterized by a quite similar shape (Fig. 1). Titanium oxide (a narrow line at 529.8 eV) and oxygen-containing groups on the surface (broader lines at ~531.1 and 533.0 eV) give the main contribution in these spectra. Oxygen-containing groups of GO also contribute to the two latter mentioned states of O 1s XPS spectra of TiO<sub>2</sub>-GO samples. The bond C-O-Ti that is formed by the dehydration reaction between -OH groups on the surface of TiO<sub>2</sub> and -OH groups of GO sheets is represented by the improvement of the charge transport properties of semiconductor; it also provides the narrowing of the band gap that is efficient for the use in photocatalysis and solar cells [20, 23].

SEM and TEM images of nanocomposite material, and SEM images of the initial components are

given in Fig. 2. It is seen that the titanium dioxide particles tend to aggregate. Graphene oxide is characterized by a layered structure that is formed by the individual sheets. The graphene oxide sheets form “wrinkles” and folds. GO sheets “coat” TiO<sub>2</sub> particles in TiO<sub>2</sub>-GO nanocomposite.

The obtained data show that the semiconductor's particles are concentrated along the folds of GO sheets. This can be related to the higher concentration of the preserved oxygen-containing groups on such regions because the interaction between graphene oxide and titanium dioxide passes via these groups [24]. This conclusion was also proven by the XPS data (see above).

The registration of the absorption spectra showed that the TiO<sub>2</sub>-GO composite can absorb much more visible light than pure titanium dioxide (Fig. 3a).

Table 1. Values of integrated areas below the XPS curves of the oxygen-containing groups in the synthesized samples

Sample	C-O, 286.6 eV	C=O, 288.4 eV	O-H/C-O, 532.5 eV
TiO <sub>2</sub>	0.94	0.78	0.52
TiO <sub>2</sub> -GO	0.30	0.23	0.67
GO	1.95	0.94	2.06

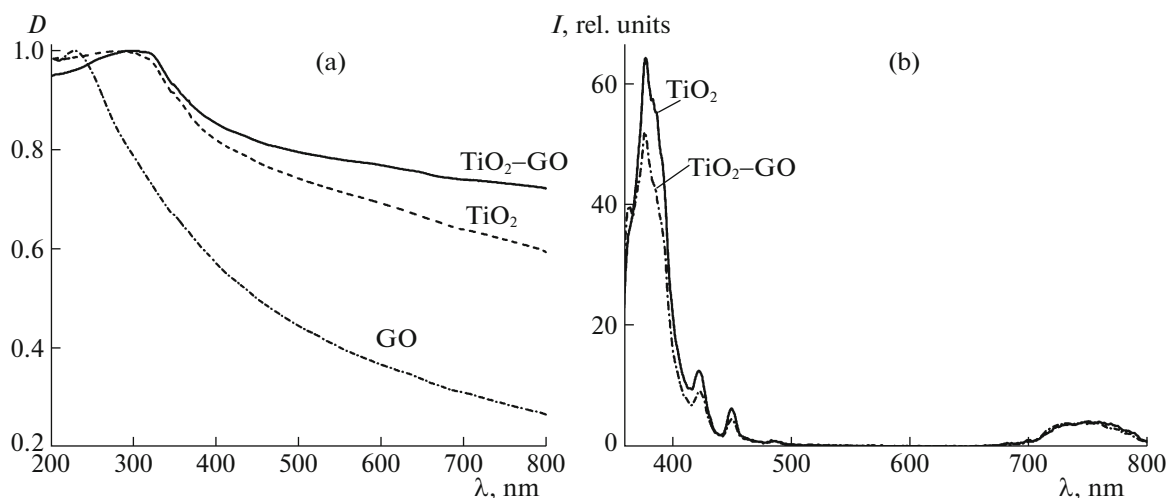


Fig. 3. Normalized absorption spectra (a) and luminescence spectra (b) of the films based on  $\text{TiO}_2$ , GO, and  $\text{TiO}_2$ -GO.

At this, the edge of the absorption band of nanocomposite is bathochromically shifted with respect to the band attributed to  $\text{TiO}_2$ , evidencing the narrowing of the band gap of the composite material. The band gap of  $\text{TiO}_2$ -GO composite decreased from 3.26 eV ( $\text{TiO}_2$ ) to 2.55 eV ( $\text{TiO}_2$ -GO); this allows this material to absorb a drastically higher number of photons and transform them into photocurrent.

Luminescence spectra are usually widely used to study the efficiency of generation, transport, and trapping of the charge carriers, and to investigate the evolution of the electron-hole pairs (EHP) in semiconductors. Photons are emitted at the recombination of EHP after irradiation of a semiconductor; photon energy can be associated with the process of deactivation of the excited states of the groups on the surface or in the volume of  $\text{TiO}_2$ . The luminescence spectra of  $\text{TiO}_2$  and  $\text{TiO}_2$ -GO films registered at the room temperature under photoexcitation of the samples by the light ( $\lambda = 330$  nm) are given in Fig. 3b. It is seen that the luminescence bands of the pure semiconductor and nanocomposite are characterized by the same shape. Several maxima can be marked out in the luminescence spectrum. The most intensive one corresponds to 380 nm; two less intensive maxima represented as the shoulders at 362 and 385 nm are located to the right and to the left from the most intensive one. Two maxima characterized by low intensity are clearly seen near 423 and 450 nm on the longwave wing of the radiation spectrum; these maxima are attributed to the traps on the oxygen vacancies characterized by the different energy. The band with the maximum at  $\sim 750$  nm was registered in the near-IR range between 700 and 800 nm; various authors attribute this band to the luminescence of the rutile form of titanium dioxide [25, 26]. The luminescence at  $\sim 360$  nm is related to the direct band gaps in semiconductor [26], while the luminescence at  $\sim 385$  and 380 nm is caused by the

indirect band gaps. At the same time, in [25], it was mentioned that this luminescence is related to the luminescence of the anatase form of  $\text{TiO}_2$  crystals; this is of the exciton nature.

The phase composition of the samples based on titanium dioxide was proven by the data of the X-ray diffraction (XRD) analysis of  $\text{TiO}_2$  and  $\text{TiO}_2$ -GO nanocomposite in the study [5]. It was shown that  $\text{TiO}_2$  nanoparticles preserve the structure of the crystal lattice after hydrothermal synthesis. The peaks typical for the crystal planes of the anatase form of  $\text{TiO}_2$  were registered in the XRD spectrum. Besides, characteristic diffraction peaks attributed to (101) and (111) planes of  $\text{TiO}_2$  rutile emerged in the spectrum at  $37.0^\circ$  and  $38.5^\circ$ .

High-energy and intensive luminescence observed in all samples can be classified as the radiative recombination of the autolocalized excitons in the volume of anatase  $\text{TiO}_2$ . Figure 3b shows that this luminescence is significantly quenched (by  $\sim 25\%$ ) in the film based on  $\text{TiO}_2$ -GO. The intensity of luminescence at 750 nm almost did not change. The thickness of the films was the same; it was controlled by both similar conditions of the film deposition and optical density value. Therefore, we can suppose that the processes of recombination of the photogenerated EHP would pass less efficiently.

We studied photoelectric parameters of the films based on  $\text{TiO}_2$  and  $\text{TiO}_2$ -GO to prove this supposition. The CVC of the studied films are given in Fig. 4. It is seen that the photocurrents registered without the light irradiation of the samples are significantly lower than the light CVC. Thus, the value of the dark current of the pure semiconductor equals 0.81 and 1  $\mu\text{A}$  at the voltage of 30 and  $-30$  V, respectively. In case of the samples containing GO this parameter equals 3.5 and 2.3  $\mu\text{A}$ , respectively. The values of photocurrent

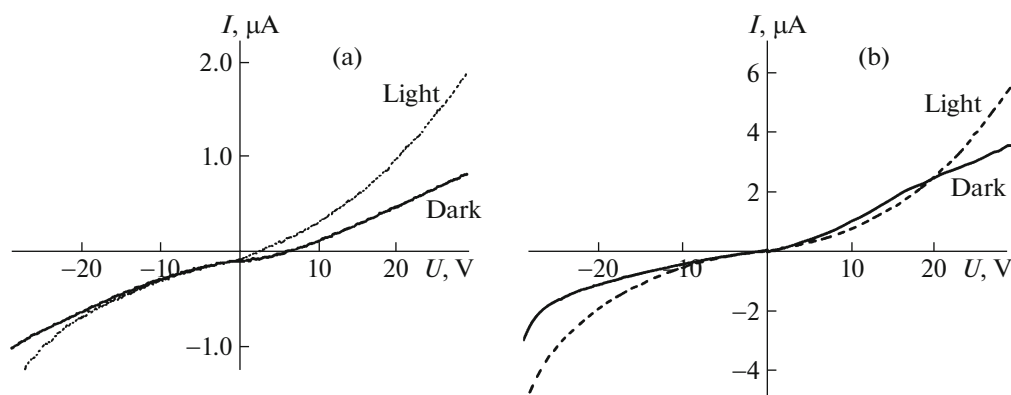


Fig. 4. Current–voltage characteristics of TiO<sub>2</sub> (a) and TiO<sub>2</sub>–GO (b).

increase for both types of films at the light irradiation. The maximum values of  $I$  equal to 1.90 and 1.24  $\mu\text{A}$ , respectively, were registered for titanium dioxide at the applied voltage of +30 and –30 V, respectively.

In the case of the nanocomposite, the values of current equaled 5.48 and 3.0  $\mu\text{A}$ , respectively. The values of generated photocurrent  $I_{\text{ph}}$  calculated as the difference between dark and light values of  $I$  are given in Table 2.

The obtained data show that significant dark currents are registered for both types of samples; it is known that dark currents are related to the electron transport in the system [27, 28]. Therefore, the corresponding high values of  $I_{\text{dark}}$  registered for TiO<sub>2</sub>–GO are determined by the increase of the number of electrons in the nanocomposite, as has been supposed above.

Sensitivity  $R$  of the prepared films was estimated using the formula  $R = I_{\text{ph}}/P$ , where  $P$  is the power of the incident radiation. The data given in Table 1 show that the sensitivity of the composite films is by 80% higher than the one of the films based on pure TiO<sub>2</sub>. As was mentioned in the studies [5, 29], the increase of photoelectric parameters of TiO<sub>2</sub>–GO can be related to either improvement of charge transport characteristics of the synthesized films or additional transfer of photogenerated electrons from GO to TiO<sub>2</sub>. At this, the oxygen vacancies on the semiconductor's surface act as the paths for electron transfer.

The specific detectivity  $D^*$  of the prepared samples was further examined; this determines the ability of a device to detect weak light signals.  $D^*$  can be determined from the following equation [30, 31]:

$$D^* = \frac{RA^{1/2}}{\sqrt{2eI_{\text{dark}}}},$$

where  $R$  is the sensitivity of films,  $A$  is the sample's area under light irradiation,  $e$  is the modulus of electron charge, and  $I_{\text{dark}}$  is the value of the dark current at +30 V. The obtained  $D^*$  values equal  $\sim 6 \times 10^7$  Jones

for both types of films; this can be explained by a higher value of the dark current in nanocomposite film as compared to pure TiO<sub>2</sub>. The comparison of the values of photocurrent,  $R$  and  $D^*$  with the data obtained by other authors [32, 33] allows marking out that the values obtained for TiO<sub>2</sub>–GO films are not inferior to the ones obtained for the pure graphene; the values of generated  $I_{\text{ph}}$  are even superior.

Photovoltaic parameters of the Grätzel cells based on the obtained nanocomposite material and TiO<sub>2</sub> are given in Table 3. The following parameters were determined on the basis of the current–voltage characteristics of solar cells: short-circuit current  $I_{\text{sc}}$ , open-circuit voltage  $V_{\text{oc}}$ , fill factor of cell  $FF$ , and cell's efficiency  $\eta$ .

The measurements showed that the introduction of 5 wt % graphene oxide additive leads to the significant worsening of the photovoltaic parameters of solar cells. However, the efficiency of the cell can be significantly improved by decreasing the mass fraction of GO in the semiconductor's film. The solar cell efficiency increases by  $\sim 2.5$  times at GO concentration of 1 wt % as compared to the efficiency registered at 5 wt % GO concentration. If we compare the parameters of cells based on nanocomposite material and pure TiO<sub>2</sub>, then it should be mentioned that the improvement of efficiency is generally determined by the increase of fill factor and value of short-circuit current.

Photoelectric parameters of solar cells were studied according to the technique given in [9, 33] based on

Table 2. Optoelectronic parameters of films based on TiO<sub>2</sub> and TiO<sub>2</sub>–GO

Sample	$I_{\text{ph}}$ , $\mu\text{A}$ at +30 V	$I_{\text{ph}}$ , $\mu\text{A}$ at –30 V	$R \times 10^{-6}$ , A/W	$D^* \times 10^{-7}$ , Jones
TiO <sub>2</sub>	1.09	0.24	31	6.3
TiO <sub>2</sub> –GO	1.98	1.3	56	6.2

**Table 3.** Photovoltaic parameters of solar cells based on TiO<sub>2</sub> and TiO<sub>2</sub>–GO

Sample	$I_{sc}$ , mA/cm <sup>2</sup>	$V_{oc}$ , mV	$FF$	Efficiency, %
TiO <sub>2</sub>	7.61	698.5	0.32	1.80
TiO <sub>2</sub> –GO 5 wt %	2.98	609.0	0.61	1.12
TiO <sub>2</sub> –GO 1 wt %	7.99	621.2	0.57	2.72
TiO <sub>2</sub> –GO 0.5 wt %	6.34	612.7	0.53	2.09

**Table 4.** Electron transport parameters of solar cells based on TiO<sub>2</sub> and TiO<sub>2</sub>–GO

Samples	$R_k$ , Ω	$R_w$ , Ω	$k_{eff}$ , s <sup>-1</sup>	$\tau_{eff}$ , ms
TiO <sub>2</sub>	265.7	33.0	51.767	19.31
TiO <sub>2</sub> –GO 0.5 wt %	509.1	47.3	37.283	26.82
TiO <sub>2</sub> –GO 1 wt %	81.2	30.9	193.03	5.180
TiO <sub>2</sub> –GO 5 wt %	142.9	33.0	372.74	2.683

$R_k$  is the charge transfer resistance related to the electron–hole recombination,  $R_w$  is the electron transport resistance in TiO<sub>2</sub>–GO film,  $k_{eff}$  is the effective recombination rate of the charge carriers, and  $\tau_{eff}$  is the electron effective lifetime.

impedance hodographs to explain the obtained data (Table 4).

The data given in Table 4 show that the addition of GO in certain concentrations into titanium dioxide films leads to a decrease of both charge transport resistance and recombination processes in the semiconductor, as has been observed in the luminescence spectrum of nanocomposite. Particularly, the value of parameter  $R_k$  decreased by 2.3 and 1.8 times for the cells containing 1 and 5 wt % of GO, respectively. At the same time, the highest value of the effective recombination rate of the charge carriers was registered for the nanocomposite containing the highest GO concentration. In the case of the GO concentration in TiO<sub>2</sub> equal to 0.5 wt %, the recombination of charge carriers passes more efficiently; however, this is compensated by a larger lifetime of the electron. Therefore, the registered parameters of solar cell efficiency are relatively high.

Thus, the influence of graphene oxide addition on the structural, optical, optoelectronic, and photovoltaic properties of TiO<sub>2</sub> was studied. It was shown that nanocomposite material is formed during hydrothermal synthesis; at this, the semiconductor's particles are concentrated along the folds of GO sheets. It can be related to the fact that a higher number of oxygen-containing groups required for the interaction between graphene oxide and titanium dioxide is preserved in these regions.

The measurements of the optical characteristics of the synthesized material showed that the absorption spectrum of TiO<sub>2</sub>–GO nanocomposite is shifted to the longwave region as compared to the absorption spectra of the initial components possibly due to the change of the band gap of semiconductor. Intensive luminescence observed in the luminescence spectra of titanium dioxide at 380 nm is related to the radiative recombination of the autolocalized excitons in the volume of anatase TiO<sub>2</sub>. GO addition leads to the ~25% quenching of luminescence evidencing the lower efficiency of the processes of recombination of the photo-generated EHP in composite. In turn, it influences the improvement of both optoelectronic characteristics of TiO<sub>2</sub>–GO films (by ~80% as compared to the pure TiO<sub>2</sub>) and their photovoltaic and electrophysical parameters.

The obtained results can be used for the elaboration of photoelectric devices and solar cells, as well as the processes of photocatalytic degradation of organic compounds.

#### FUNDING

This study was supported by the Ministry of Education and Science of the Republic of Kazakhstan (projects BR05236691 and AP05132443).

#### CONFLICT OF INTEREST

We have no conflicts of interest to declare.

#### REFERENCES

1. N. I. Zaaba, K. L. Hashima, U. Foo, et al., *Solv. Infl. Proc. Eng.* **184**, 469 (2017).
2. M. S. A. Bhuyan, M. N. Uddin, and M. M. Islam, *Int. Nano Lett.* **6**, 65 (2016).
3. E. V. Seliverstova, N. Kh. Ibrayev, and R. Kh. Dzhanabekova, *Bull. KazNU, Chem. Ser., No. 3 (79)*, 67 (2015).
4. E. V. Seliverstova, N. Kh. Ibrayev, and R. Kh. Dzhanabekova, *Nanosyst.: Phys., Chem., Math., No. 7 (1)*, 65 (2016).
5. N. Ibrayev, A. Zhumabekov, S. Ghyngazov, and E. Lysenko, *Mater. Res. Express* **6**, 125036 (2019).
6. Y. M. Shulga, A. V. Melezhik, E. N. Kabachkov, et al., *High Energy Chem., No. 57 (1)*, 47 (2019).
7. Ch. Chen, W. Cai, M. Long, et al., *ACS Nano* **4**, 6425 (2010).
8. A. N. Fouda, A. B. El Basaty, and E. A. Eid, *Nano Res. Lett.* **11**, 13 (2016).
9. A. Zh. Zhumabekov, N. Kh. Ibrayev, and E. V. Seliverstova, *Theor. Exp. Chem.* **55**, 398 (2020).
10. X. Yu, Y. Li, and X. Hu, *Nat. Commun.* **9**, 4299 (2018).
11. N. Nuraje, R. Asmatulu, and G. Mul, *Green Photo-Active Nanomaterials: Sustainable Energy and Environment Remediation* (R. Soc. Chem., Cambridge, 2015).

12. S. Sharma, S. Bulkesh, S. K. Ghoshal, et al., *Renew. Sustain. Energy Rev.* **70**, 529 (2017).
13. S. Daulay, A. F. Madsuha, E. S. Rosa, et al., *J. Phys.: Conf. Ser.* **1402**, 055101 (2019).
14. Y. Zhang, H. Li, L. Kuo, et al., *Curr. Opin. Colloid Interface Sci.* **20**, 406 (2015).
15. A. Eshaghi and A. Ail Aghaei, *Bull. Mater. Sci.* **38**, 1177 (2015).
16. M. F. Zulkapli, N. M. Rashid, M. Nazri, et al., *Environ. Ecosyst. Sci.* **2** (2), 39 (2018).
17. S. A. Kazmi, S. Hameed, A. S. Ahmed, et al., *J. Alloys Compd.* **691**, 659 (2017).
18. B. Pant, P. S. Saud, M. Park, et al., *J. Alloys Compd.* **671**, 51 (2016).
19. N. Kh. Ibrayev, E. V. Seliverstova, A. A. Ishchenko, and M. A. Kudinova, *J. Photochem. Photobiol., A* **306**, 570 (2017).
20. B. O'Regan and M. Gratzel, *Nature (London, U.K.)* **353**, 737 (1991).
21. J. Zhang, X. Xu, H. Yang, et al., *Environ. Technol.* **42** (2), 193 (2021).
22. L. Zhang, J. Zhang, H. Jiu, et al., *J. Phys. Chem. Solids* **86**, 82 (2015).
23. Y. Chen, H. Gao, and J. Xiang, *Mater. Res. Bull.* **99**, 29 (2018).
24. M. Manzoor, A. Rafiq, M. Ikram, et al., *Int. Nano Lett.* **8**, 1 (2018).
25. S. A. Abdullah, M. Z. Sahdan, and N. Nafarizal, *IOP Conf. Ser.: J. Phys.* **995**, 012067 (2018).
26. D. Nadica, M. I. Abazović, and M. D. Čomor, *J. Phys. Chem.* **110**, 25366 (2006).
27. D. Zhang, F. Jing, and F. Gao, *RSC Adv.* **5**, 83795 (2015).
28. A. Balducci, M. Marinelli, E. Milani, et al., *Appl. Phys. Lett.* **86**, 193509 (2005).
29. D. H. Shin and S.-H. Choi, *Micromachines* **9**, 350 (2018).
30. Sh. Li, D. Tao, Ya. Zhang, et al., *Nanophotonics* **8**, 899 (2019).
31. A. de Sanctis, J. D. Mehew, M. F. Craciun, et al., *Materials* **11**, 1762 (2018).
32. V. Patil, A. Capone, S. Strauf, et al., *Sci. Rep.* **3**, 2791 (2013).
33. J. Bisquert, *J. Phys. Chem. B* **106**, 325 (2002).

*Translated by P. Vlasov*